Substrate-induced spin-torque-like signal in spin-torque ferromagnetic resonance measurement

Dingsong Jiang,[1,‡] Hetian Chen,[2,‡] Guiping Ji,[1] Yahong Chai,[1] Chenye Zhang,[1] Yuhan Liang,[2] Jingchun Liu,[2] Witold Skowroński,[3] Pu Yu,[4] Di Yi,[2,*] and Tianxiang Nan[1,†]

[1] *School of Integrated Circuit and Beijing National Research Center for Information Science and Technology (BNRist), Tsinghua University, Beijing, China*

[2] *School of Materials Science and Engineering, Tsinghua University, Beijing, China*

[3] *AGH University of Krakow, Institute of Electronics, Kraków, Poland*

[4] *Department of Physics, Tsinghua University, Beijing, China*

(Received 6 August 2023; revised 18 December 2023; accepted 10 January 2024; published 9 February 2024)

Oxide thin films and interfaces with strong spin-orbit coupling have recently shown exceptionally high charge-to-spin conversion, making them potential spin-source materials for spintronics. Epitaxial strain engineering using oxide substrates with different lattice constants and symmetries has emerged as a mean to further enhance charge-to-spin conversion. However, high relative permittivity and dielectric loss of commonly used oxide substrates, such as $SrTiO_3$, can cause significant current shunting in substrates at high frequency, which may strongly affect spin-torque measurement and potentially result in an inaccurate estimation of charge-to-spin conversion efficiency. In this study, we systematically evaluate the influence of various oxide substrates for the widely used spin-torque ferromagnetic resonance (ST-FMR) measurement. Surprisingly, we observed substantial spin-torque signals in samples comprising only ferromagnetic metal on oxide substrates with high relative permittivity (e.g., $SrTiO_3$ and $KTaO_3$), where negligible signal should be initially expected. Notably, this unexpected signal shows a strong correlation with the capacitive reactance of oxide substrates and the leakage rf current within the substrate. By revising the conventional ST-FMR analysis model, we attribute this phenomenon to a 90° phase difference between the rf current flowing in the metal layer and in the substrate. We suggest that extra attention should be paid during the ST-FMR measurements, as this artifact could dominate over the real spin-orbit torque signal from high-resistivity spin-source materials grown on substrate with high relative permittivity.

DOI: 10.1103/PhysRevApplied.21.024021

I. INTRODUCTION

Magnetic random-access memories (MRAMs) and spintronic logical devices based on spin-orbit torques (SOTs) have garnered significant research attention due to their low-power consumption, high endurance, high-speed, and nonvolatile properties [1–10]. The development of materials capable of generating SOT with high-efficiency and the establishment of accurate metrologies for quantifying current-induced SOTs in various material systems are crucial. To evaluate SOT efficiency of spin-source materials, several experimental techniques have been devised to detect static or dynamic changes in magnetization of ferromagnet (FM) induced by SOTs [11]. These methods include spin-torque ferromagnetic resonance (ST-FMR) [12–17], second-harmonic Hall voltage (SHHV) [18–20], measurements of current-induced hysteresis-loop shift [21–23], measurements of current-induced magnetization switching [24], and optical measurements of current-induced effective field [25–27], etc. Among these techniques, ST-FMR stands out as a widely employed method for measuring SOTs due to its self-calibration, simplicity, and versatility across a wide range of material systems [12–14,28–31]. ST-FMR allows the examination of magnetization dynamics induced by SOTs at ferromagnetic resonance frequencies of the gigahertz range, providing insights into both dampinglike and fieldlike SOTs. During the ST-FMR measurements, spin pumping from the magnetic layer to the spin-source layer, coupled with the inverse spin-Hall effect, can contribute to the spin-torque signal and is considered as the major source of artifact, which has been carefully evaluated [31,32]. On the other hand, despite considerable attention paid to the fact that substrates could become highly conductive at high frequencies and generate spin-torque-like signals, the impact

*diyi@mail.tsinghua.edu.cn

†nantianxiang@mail.tsinghua.edu.cn

‡The authors contribute equally to this work.

of substrates to the ST-FMR measurements has not been thoroughly investigated.

Remarkably, the influence of substrates could be even more pronounced when measuring SOTs in oxide spin-source materials, which have recently exhibited an exceptionally strong spin-Hall effect [28,30,33–36]. Firstly, oxide spin-source materials typically have higher resistivity compared to heavy metals at room temperature (i.e., Pt $\sim$ 20 μΩcm [12], $SrIrO_3$ $\sim$ 570 μΩcm [37], $SrRuO_3$ $\sim$ 290 μΩcm [36]). Secondly, oxide substrates, such as $SrTiO_3$ and $KTaO_3$, which are commonly employed for epitaxial growth of oxide spin sources [15, 29,30,35,36] and two-dimensional electron-gas (2DEG) systems [33,38–40], exhibit high conductivity at high frequencies due to their high dielectric constant and dielectric loss [41,42]. This combination leads to a much more pronounced rf current shunting effect from the substrate in oxide spin sources as compared to heavy-metal materials in ST-FMR measurements.

In this work, we investigated the artifact spin-torque signal in ST-FMR measurements on different oxide substrates with a wide range of relative permittivity. We find that the artifact spin-torque signal is large in samples of only ferromagnetic metal permalloy (Py) on oxide substrates with high relative permittivity (without a spin-source material). This artifact spin-torque signal is inversely proportional to the capacitive reactance of substrates, which can be attributed to the Oersted field generated by an off-phased leakage rf current in oxide substrates according to our revised ST-FMR analysis model. Notably, we demonstrate that this artifact spin-torque signal can significantly impact the spin-Hall ratio analysis of Pt, a benchmarked spin-Hall source material with high conductivity, when using $SrTiO_3$ substrate. When using the more resistive oxide spin-Hall source materials, such as $SrIrO_3$, the spin-torque signal from $SrIrO_3$ could be overwhelmed by the artifact from $SrTiO_3$ alone. Our findings offer a deeper insight into the origin of spin-torque signal measured in oxide spin-Hall sources and pave the way for a more precise measurement of SOT materials.

II. SPIN-TORQUE FERROMAGNETIC RESONANCE

In ST-FMR measurements, a microwave rf current is applied on the microstrip of spin-Hall source material/FM bilayer. Due to the spin-Hall effect (SHE) [43] or Rashba-Edelstein effect (REE) [44], an rf spin current is generated in the spin-Hall source layer and inject into the adjacent FM layer to induce a magnetization precession, which leads to an oscillation of the microstrip resistance because of the anisotropic or spin-Hall magnetoresistance in the FM layer. The ST-FMR voltage signal can be detected by mixing the rf current with the oscillating resistance [12,13,45]. By solving the Landau-Lifshitz-Gilbert (LLG) equation, one can obtain the mixing voltage as a function of the external magnetic field [12,13,31], as expressed in Eq. (1):

$$V_{\mathrm{mix}}(H_{\mathrm{ext}}) = V_S \frac{\Delta H^2}{\Delta H^2 + (H_{\mathrm{ext}} - H_0)^2} + V_A \frac{\Delta H (H_{\mathrm{ext}} - H_0)}{\Delta H^2 + (H_{\mathrm{ext}} - H_0)^2}, \tag{1}$$

where H_{ext} is the external magnetic field, ΔH and H_0 are the linewidth and resonance field, respectively. By employing the fitting procedure of Eq. (1) consisting of symmetric and antisymmetric Lorentzian functions to the experimental data, two voltage components can be extracted: a symmetric voltage component V_S proportional to the strength of the dampinglike torque τ_{DL}, and an antisymmetric voltage component V_A proportional to the strength of the sum of fieldlike torque τ_{FL} and rf Oersted field H_{rf}, according to Eqs. (2) and (3), respectively:

$$V_S = -\frac{1}{4}\frac{dR}{d\varphi}\frac{I_{\mathrm{rf}}\cos\varphi}{2\pi\,\Delta H (df/dH_{\mathrm{ext}})|_{H_{\mathrm{ext}}=H_0}}\tau_{\mathrm{DL}}, \tag{2}$$

$$V_A = -\frac{1}{4}\frac{dR}{d\varphi}\frac{I_{\mathrm{rf}}\cos\varphi\sqrt{1+(4\pi M_{\mathrm{eff}}/H_0)}}{2\pi\,\Delta H (df/dH_{\mathrm{ext}})|_{H_{\mathrm{ext}}=H_0}}(\tau_{\mathrm{FL}} + \gamma\mu_0 H_{\mathrm{rf}}), \tag{3}$$

where f is the excitation frequency of ST-FMR measurement, γ is the gyromagnetic ratio, μ_0 is the permeability in vacuum, R is the resistance of microstrip, I_{rf} is the RF current through the microstrip, $4\pi M_{\mathrm{eff}}$ is the effective demagnetization field, φ is the angle between I_{rf} and H_{ext}. Finally, the spin-Hall ratio θ_{SH} can be calculated via [15,45]:

$$\theta_{\mathrm{SH}} = \tau_{\mathrm{DL}}\frac{2e}{\hbar}\frac{M_S t l \rho}{I_{\mathrm{rf}} R}, \tag{4}$$

where $\hbar$ is the reduced Planck's constant, e is the electron charge, l is the length of the microstrip, t is the thickness of FM layer, ρ is the resistivity of spin-Hall source layer. In Eq. (4), the only unknown parameter is the rf current I_{rf}, which can be measured using a vector-network analyzer [45,46]. Alternatively, in a simpler scenario, the spin-Hall ratio θ_{SH} can be estimated by considering the ratio of V_S to V_A, denoted as

$$\theta_{\mathrm{SH}} = (V_S/V_A)(e\mu_0 M_s t d)/\hbar\sqrt{1+4\pi M_{\mathrm{eff}}/H_0},$$

assumming that V_A is primarily contributed from the Oersted field, where d is the thickness of spin-Hall source layer [12,29,30]. It should be noted that in systems with significant fieldlike torques [17,47,48], the spin-Hall ratio

obtained solely from the ratio of V_S to V_A may lead to misestimations. Nevertheless, accurate measurements of the symmetric component (V_S) are of great significance for determination of the spin-Hall ratio in ST-FMR measurements.

III. DEVICE PREPARATION AND MEASUREMENTS

In this study, we used oxide substrates with different relative permittivity ε_r at room temperature during the ST-FMR measurements. The substrates used were 5×5 mm^2, 500-μm-thickness (001)-oriented $SrTiO_3$ (STO, $\varepsilon_r \sim 300$ [41]), (001)-oriented $KTaO_3$ (KTO, $\varepsilon_r \sim 290$ [42]), (001)-oriented $(LaAlO)_{0.3}$-$(Sr_2AlTaO_6)_{0.7}$ (LSAT, $\varepsilon_r \sim 22.6$ [50]), (110)-oriented $DyScO_3$ (DSO, $\varepsilon_r \sim 26$ [51]), and (0001)-oriented Al_2O_3 ($\varepsilon_r \sim 9.2$ [52]), and all substrates were not treated with any solutions. To make the samples without any spin-Hall source materials, we deposited only the ferromagnetic thin films of Py (5 nm) capped with Ti (1.5 nm) onto these oxide substrates by using high-vacuum magnetron sputtering at an Ar pressure of 3 mTorr. To make the control samples, bilayers of Pt(5 nm)/Py(5 nm) and Py(5 nm)/Pt(5 nm) with reversed layered sequence were deposited on STO, and Pt(5 nm)/Py(5 nm) was deposited on Si($\rho \sim 0.01$ Ω cm)/SiO_2(500 nm). For samples with oxide spin-Hall-source materials, 17-nm $SrIrO_3$ (SIO) was grown on a (001)-oriented STO substrate by using a pulsed-laser deposition (PLD) with a 248-nm KrF excimer laser at an oxygen pressure of 0.1 Torr. During the PLD growth, the growth temperature was 700 °C, and the laser energy density was maintained at 1.2 J/cm^2. Subsequently, the sample was cooled to room temperature in an oxygen atmosphere of 30 Torr. Then a 5-nm Py was deposited onto the samples by sputtering. All samples were fabricated using the lithography and ion-beam etching processes, into the 16×80 μm^2 microstripes with ground-signal-ground (GSG) electrodes for ST-FMR measurements and 16×80 μm^2 Hall bars for SHHV measurements. In particular, for the STO/Py, STO/Pt/Py, and STO/Py/Pt samples, we confirmed that the STO substrates were still insulative after the device fabrication processes by measuring the dc resistance (>200 MΩ) between two metal pads separated by approximately 200 μm.

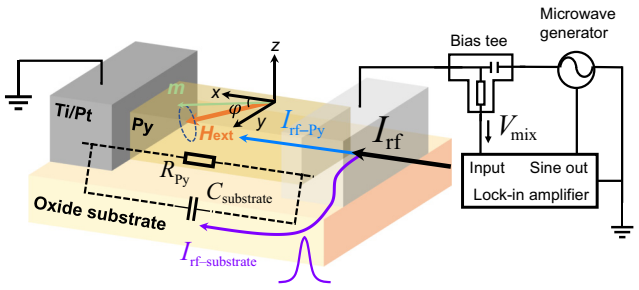

FIG. 1. Schematic of ST-FMR measurement setup and rf current shunting model. H_{ext} is the external magnetic field, φ is the angle between rf current I_{rf} and external magnetic field H_{ext}, m is the magnetization of Py layer. I_{rf}, $I_{rf-substrate}$, I_{rf-Py} are the total rf current through oxide substrate/Py device, leakage rf current in oxide substrate, and rf current in Py, respectively. R_{Py} is the equivalent resistor of Py layer, and $C_{substrate}$ is the capacitor formed in oxide substrate through the ground-signal-ground (GSG) electrode.

Figure 1 shows the schematic of ST-FMR measurement setup, in which a microwave current with a power of 15 dBm is applied on the microstrip along the $+x$ direction from a microwave generator and is modulated by a low-frequency sinewave at 1713 Hz. The mixing voltage signal was measured by a lock-in amplifier as a function of the external magnetic field H_{ext}. To characterize the impedance of samples, we used a vector-network analyzer (VNA) to measure the scattering parameter S_{11} (see Fig. S1 within the Supplemental Material [49] for a detailed description of the measurement).

IV. RESULTS

Figures 2(a)–2(e) show the typical ST-FMR spectra of 5-nm Py on substrates of STO, KTO, Al_2O_3, DSO, and LSAT measured at $f = 5$ GHz, $\varphi = 225°$, which can be well fit by the sum of symmetric and antisymmetric Lorentzian functions expressed in Eq. (1). We found that the symmetric voltage signal that was attributed to dampinglike torque appears in all five samples. Noticeably, the symmetric voltage signal from STO/Py(5 nm), KTO/Py(5 nm) has the same order of magnitude as the Si/SiO_2/Pt(5 nm)/Py(5 nm) control sample, which has a substantial dampinglike torque with a spin-Hall ratio of 0.071 ± 0.002 (see Fig. S2 within the Supplemental Material [49] for details). However, in all samples including STO/Py and KTO/Py, the dampinglike torque should be negligible since there is no spin-source layer [12], as confirmed by an independent low-frequency SHHV measurements (see Fig. S3 within the Supplemental Material [49] for details of SHHV measurements). The discrepancy between ST-FMR and SHHV measurements for the oxide substrate/Py devices (especially the heterostructures of STO/Py and KTO/Py) implies that the symmetric signal from ST-FMR measurements is not originated from SOT but might be an artifact signal. Furthermore, we discovered that this artifact signal possessed the same symmetry as that of SOT, with the same angular dependence as Si/SiO_2/Pt/Py control sample (see Fig. S6 within the Supplemental Material [49]). Additionally, small antisymmetric components are also observed from all oxide substrate/Py samples, which could be originated from a fieldlike torque due to the Rashba effect at the Py/Ti interface [53].

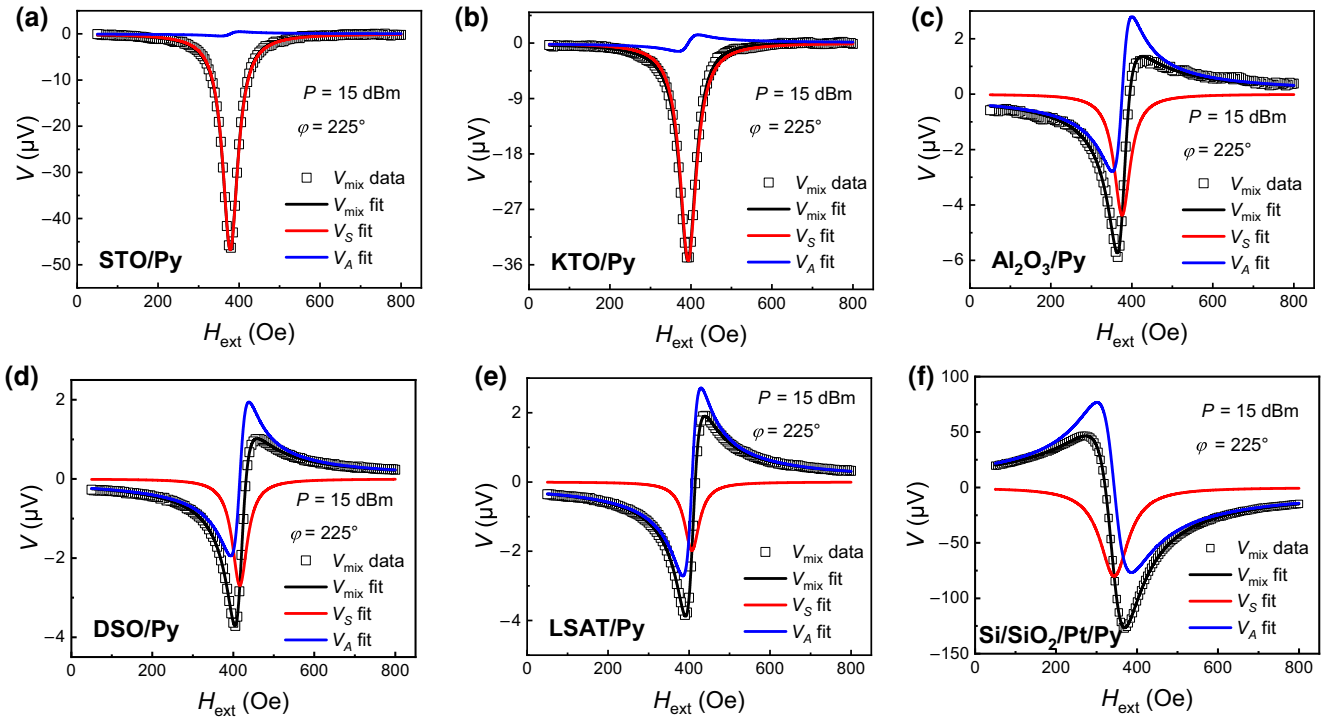

FIG. 2. The typical ST-FMR spectra of (a) STO, (b) KTO, (c) Al_2O_3, (d) DSO, (e) LSAT oxide substrate/Py(5 nm) devices, and (f) Si/SiO_2/Pt(5 nm)/Py(5 nm) device at $f = 5$ GHz, $\varphi = 225°$, $P = 15$ dBm. The black hollow squares represent the experimental data. The black lines, red lines, and blue lines are the sum of symmetric and antisymmetric Lorentz functions fitting V_{mix}, symmetric Lorentzian function fitting V_S, and antisymmetric Lorentzian function fitting V_A, respectively.

To understand the origin of the artifact symmetric voltage signal observed in ST-FMR measurements, we established a revised ST-FMR analysis model by considering the leakage rf current in oxide substrates. As shown in Fig. 1, the device can be considered as a resistance R_{Py} of Py and a capacitor $C_{\mathrm{substrate}}$ formed between two electrodes that are connected in parallel. At the frequency of ST-FMR measurement (5–10 GHz), the capacitive reactance of $C_{\mathrm{substrate}}$ decreases as the frequency increases, and thereby the substrates might become conductive at radiofrequencies. As a result, part of the rf current will flow through the oxide substrate due to the current shunting. Therefore, as shown in Fig. 1, the total rf current I_{rf} through the oxide substrate/Py device consists of two components: the rf current $I_{\mathrm{rf-Py}}$ through R_{Py}, and the rf current $I_{\mathrm{rf-substrate}}$ through $C_{\mathrm{substrate}}$. Similar to the conventional spin-Hall source material/FM bilayer, $I_{\mathrm{rf-substrate}}$ in the oxide substrate will generate an rf Oersted field H'_{rf}, as shown in Fig. 3(a). However, the fieldlike torque of Oersted field would generally give rise to an antisymmetric signal [12], which cannot explain the artifact symmetric signal we observed. It should be noted that there is a 90° phase difference between $I_{\mathrm{rf-Py}}$ and $I_{\mathrm{rf-substrate}}$, as shown in Fig. 3(b). Thereby, due to the 90° phase difference between the symmetric and antisymmetric signals, the off-phased H'_{rf} generated from $I_{\mathrm{rf-substrate}}$ would cause the appearance of the artifact symmetric signal.

To account for this signal, we revised the ST-FMR analysis model starting with the LLG equation to get the mixing voltage of oxide substrate/Py (see Fig. S4 within the Supplemental Material [49] for details). The revised mixing voltage is then expressed as Eq. (5):

$$\begin{aligned} V'_{\mathrm{mix}} &= -\frac{1}{4}\frac{dR}{d\varphi}\frac{|I_{\mathrm{rf}}|\cos\varphi}{\Delta H 2\pi df\,/dH_{\mathrm{ext}}|_{H_{\mathrm{ext}}=H_0}} \\ &\quad\times\sqrt{1+(4\pi M_{\mathrm{eff}}/H_0)}\frac{\gamma\mu_0|I_{\mathrm{rf-substrate}}|}{2w}F_S(H_{\mathrm{ext}}) \\ &= V'_S F_S(H_{\mathrm{ext}}), \end{aligned} \tag{5}$$

where w is the width of microstrip, $F_S(H_{\mathrm{ext}})$ is the symmetric Lorentzian function, V'_S is the amplitude for that symmetric signal. From Eq. (5), we could conclude that the fieldlike torque of $H'_{\mathrm{rf}} \propto I_{\mathrm{rf,substrate}}$ would actually give rise to an artifact symmetric signal V'_S in the revised model owing to the 90° phase difference between $I_{\mathrm{rf-substrate}}$ and $I_{\mathrm{rf-Py}}$. As we mentioned earlier, the symmetric signal can only be generated when there is a finite dampinglike torque from the spin-Hall source layer in the conventional ST-FMR analysis model [Eqs. (1) and (2)]. To link the artifact symmetric signal to the capacitive reactance of substrate,

we rewrite V_S' as

$$V_S' = \left[-\frac{1}{4}\frac{dR}{d\varphi}\frac{\gamma\mu_0|P|\cos\varphi}{\Delta H 2\pi df\ /dH_{\text{ext}}|_{H_{\text{ext}}=H_0}} \times \left(\sqrt{1+(4\pi M_{\text{eff}}/H_0)}\frac{1}{2w}\right)\right]\frac{1}{|\chi_{\text{substrate}}|}, \quad (6)$$

where $|P|$ is the modulus of power of the microwave used in ST-FMR measurements, which can be expressed as $|P| = |I_{\text{rf}}|^2|Z_{\text{device}}|$, and $\chi_{\text{substrate}}$ is the reactance of $C_{\text{substrate}}$, which can be expressed as $\chi_{\text{substrate}} = 1/j2\pi f\, C_{\text{substrate}}$. The part on the left side of $1/|\chi_{\text{substrate}}|$ in Eq. (6) can be approximatively regarded as a constant and thereby V_S' would show a linear dependence on $1/|\chi_{\text{substrate}}|$.

To experimentally explore the above correlation, we have first measured the impedance of oxide substrate/Py devices and bare oxide substrates by using a vector-network analyzer through the GSG electrodes at frequencies of 5–10 GHz. Due to the parallel connection, the impedance of oxide substrate/Py device Z_{device} can be expressed as Eq. (7):

$$Z_{\text{device}} = \frac{R_{\text{Py}}}{1+(2\pi f\, C_{\text{substrate}}R_{\text{Py}})^2}(1 - j2\pi f\, C_{\text{substrate}}R_{\text{Py}}). \quad (7)$$

Figure 3(c) shows the modulus of impedance for oxide substrate/Py devices and bare oxide substrates, along with the phase of impedance of the oxide substrate/Py devices. We found that $|Z_{\text{substrate}}|$ ($|\chi_{\text{substrate}}|$) decreases as $C_{\text{substrate}} \propto \varepsilon_r$ and $|Z_{\text{device}}|$ is smaller than $|Z_{\text{substrate}}|$ for different oxide substrates, and α_{device} indicated by $\alpha_{\text{device}} = \arctan(-2\pi f \times R_{\text{Py}}C_{\text{substrate}})$ being close to $-90°$ as $|Z_{\text{substrate}}|$ decreases, which indicates the parrellel connection between R_{Py} and $C_{\text{substrate}}$. Particularly, $|Z_{\text{device}}|$ becomes close to $|Z_{\text{substrate}}|$ for STO and KTO due to their high relative permittivity, suggesting that $I_{\text{rf-substrate}}$ would dominant over $I_{\text{rf-Py}}$ in STO/Py and KTO/Py devices. Figure 3(d) summarizes the measured artifact symmetric signals as a function of $1/|\chi_{\text{substrate}}|$ for different oxide substrate/Py devices at a frequency of 5 GHz (see Fig. S13 within the Supplemental Material [49] for the correlations between V_S' and $1/|\chi_{\text{substrate}}|$ at 6–10 GHz). The deviation from the linear fitting of V_S' vs $1/|\chi_{\text{substrate}}|$ for samples with small permittivity substrates at higher frequencies

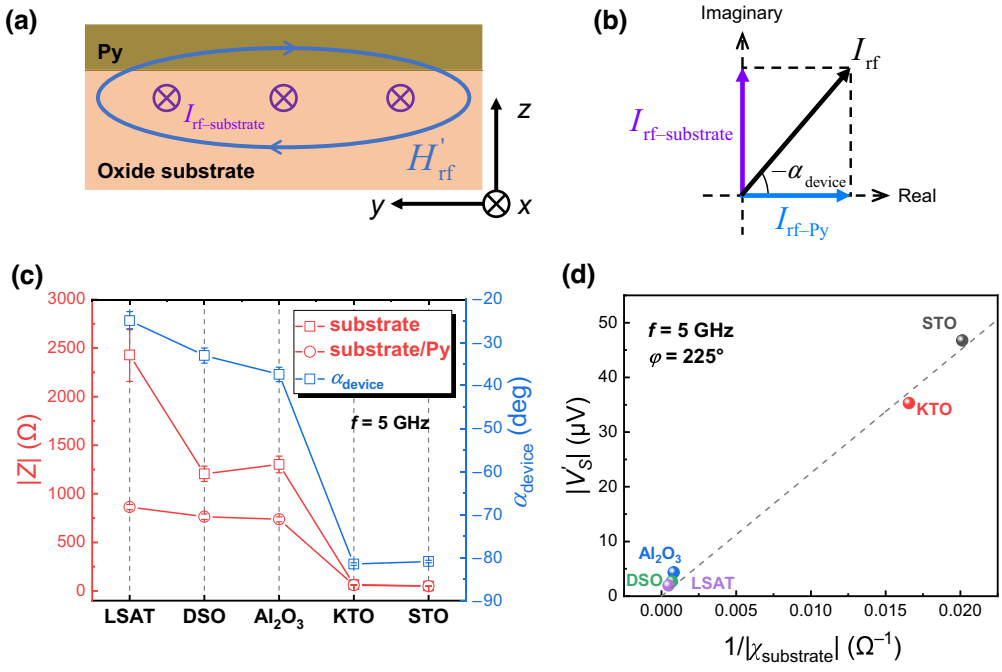

FIG. 3. (a) Sectional view of the oxide substrate/Py device. H'_{rf} is the rf Oersted field generated by the leakage rf current $I_{\text{rf-substrate}}$ in oxide substrate. (b) The relation between total rf current I_{rf}, rf current in oxide substrate $I_{\text{rf-substrate}}$, and rf current in Py $I_{\text{rf-Py}}$. The length of the arrow represents the modulus of rf current and α_{device} is the phase of impedance of the oxide substrate/Py device. (c) The modulus of impedance $|Z|$ of the different oxide substrates, oxide substrate/Py devices, and the phase of impedance α_{device} of the different oxide substrate/Py devices measured using a vector-network analyzer at $f = 5$ GHz, respectively. (d) The correlation between the absolute value of the artifact symmetric voltage signal V_S' and the capacitive reactance of oxide substrate $|\chi_{\text{substrate}}|$ at $f = 5$ GHz, $\varphi = 225°$. The dashed line is a linear fit.

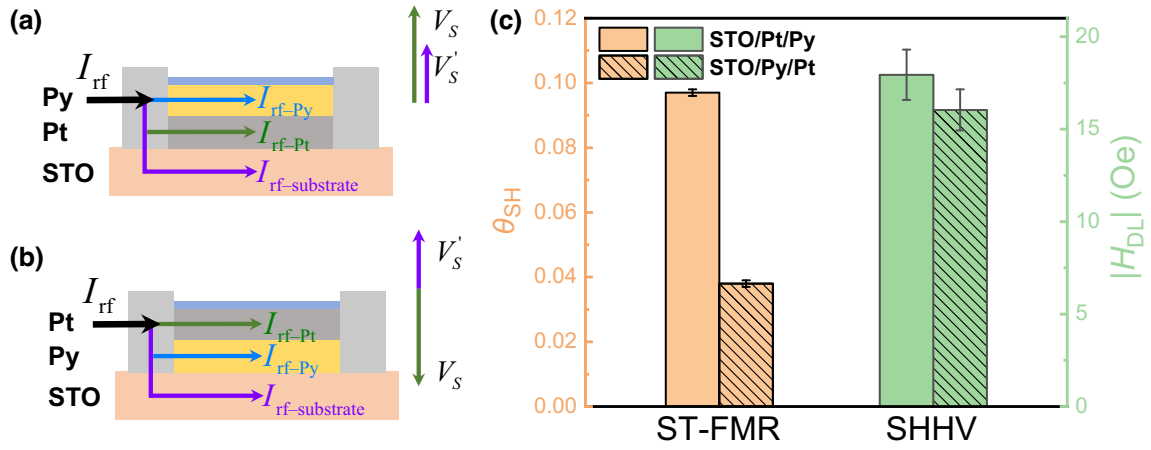

FIG. 4. Schematic of the influence of the artifact symmetric voltage on the spin-Hall ratio of Pt in (a) STO/Pt/Py and (b) STO/Py/Pt samples. I_{rf} is the total rf current. I_{rf-Py}, I_{rf-Pt}, and $I_{rf-substrate}$ are the rf current in Py, Pt, and STO substrate, respectively. V_S is the symmetric component related to the dampinglike torque from I_{rf-Pt}, V_S' is the artifact symmetric signal generated from the leakage rf current $I_{rf-substrate}$ in STO. (c) The spin-Hall ratio θ_{SH} obtained from ST-FMR measurements, along with the dampinglike effective fields H_{DL} obtained from SHHV of STO/Pt/Py and STO/Py/Pt.

shown in Fig. S13 within the Supplemental Material [49] may be attributed to some self-induced spin-torque signals from single Py and other spurious effects such as the spin pumping from Py [54,55]. As shown in Fig. 2, given the significant dependence on substrates, other self-induced effects of the single Py are negligible compared with the artifact symmetric signal arising from the leakage rf current in substrate. The observed linear relation between V_S' and $1/|\chi_{substrate}|$ is in good agreement with our model expressed as Eq. (6), providing strong evidence that the artifact symmetric voltage signal in oxide substrate/Py indeed arises from the leakage rf current in the oxide substrate.

To directly evaluate the influence of the artifact symmetric signal from oxide substrates with high relative permittivity on determining the spin-Hall ratio with the ST-FMR measurements, we prepared Pt(5 nm)/Py(5 nm) and Py(5 nm)/Pt(5 nm) with a reversed layered sequence on the STO substrate. In these samples, the total rf current I_{rf} consists of I_{rf-Py}, I_{rf-Pt} and $I_{rf-substrate}$, in which I_{rf-Pt} gives rise to a symmetric signal V_S from dampinglike torque on Py, while $I_{rf-substrate}$ gives rise to the artifact symmetric signal V_S'. As shown in Fig. 2, the artifact signal from $I_{rf-substrate}$ has the same symmetry as that from I_{rf-Pt}, which means the V_S' and V_S have the same sign when Pt and oxide substrate is on the same side of Py. However, when Pt and oxide substrate are on the opposite side of Py, V_S' and V_S would have an opposite sign and cancel out to each other. Specifically, in the STO/Pt/Py sample, V_S' from STO would add up to V_S from Pt as shown in Fig. 4(a), resulting in an overestimation of θ_{SH} for Pt; while conversely, in the STO/Py/Pt sample, V_S' would counteract V_S, as shown in Fig. 4(b), resulting in an underestimation of θ_{SH}.

Figure 4(c) shows the spin-Hall ratio θ_{SH} extracted from the ST-FMR measurements (see Fig. S5 within the Supplemental Material [49] for details). θ_{SH} is found to be 0.097 ± 0.001 for STO/Pt/Py, which is about 2.5 times larger than 0.038 ± 0.001 for STO/Py/Pt, consistent with our model. To validate our findings further, we measured the dampinglike torque of STO/Pt/Py and STO/Py/Pt by using an independent low-frequency SHHV measurements (see S5 within the Supplemental Material [49] for details). In this measurement, the leakage current in oxide substrate should be minimal since the driving frequency for the measurement is low (233 Hz). The dampinglike effective fields H_{DL} for these two samples extracted from SHHV were found to be almost the same within experimental uncertainties, as shown in Fig. 4(c). The large discrepancy of the spin-Hall ratios for these two samples using ST-FMR measurements (while almost no difference when using SHHV) demonstrates that substrates with high relative permittivity significantly influence the estimation of the spin-Hall ratio, even in spin-Hall source materials with high conductivity, in ST-FMR measurements.

V. DISCUSSION

While the self-calibrated ST-FMR measurement offers unique advantages over other spin-torque measurement techniques, it is crucial to recognize that certain substrates with high relative permittivity can introduce significant artifact spin-torque signals in ST-FMR measurement, particularly in spin-Hall source materials with high resistivity. For example, $4d/5d$ transition-metal-oxide thin films have recently exhibited exceptionally large spin-Hall ratio [15,28–30,34,37], often possess higher resistivity than heavy metals. When measuring the oxide thin films grown

on high-relative-permittivity substrates, such as STO and KTO using ST-FMR measurement, their large resistivity can lead to the majority of rf current flowing in substrate, leading to a pronounced artifact symmetric signal.

Previous studies on 4*d*/5*d* transition-metal-oxide thin films and oxide 2DEG systems have frequently used the ST-FMR technique with the analysis of the symmetric signal. Large variations in amplitude and even in sign of spin-Hall ratio have been for the same spin-Hall material with different epitaxial substrates and layered structure [15,28–30,33,37,38,56]. Our results indicate that this varation could mainly be attributed to the artifact symmetric signal caused by using substrates with high relative permittivity [Fig. 3(d)] and the sequence of heterostructures [Figs. 4(a) and 4(b)], rather than the other intrinsic mechanisms. For instance, our ST-FMR results for the STO/SIO(17 nm)/Py(5 nm) sample (see Fig. S6 in Supplemental Material [49] for details) show nearly the same magnitude of symmetric signal as compared to the STO/Py(5 nm) sample [Fig. 2(a)], indicating that the influence of artifact symmetric signal from STO is overwhelming.

We proposed that employing the dc current-tuned ST-FMR measurements [12,13,15,29] may eliminate the influence of the artifact signal from substrate since there is no obvious correlation between the artifact symmetric signal and the current-induced change of linewidth [see Fig. S7(b) within the Supplemental Material [49]]. Furthermore, spin-torque measurement techniques at quasistatic frequencies, such as SHHV [29,57,58] or current-induced loop shift [21–23], should be adopted when characterizing the spin-Hall materials with high resistivity on substrate with high permitivity.

VI. CONCLUSIONS

In conclusion, we have uncovered the presence of a significant artifact symmetric signal in ST-FMR measurements of oxide substrate/Py devices. By revising the conventional ST-FMR analysis model, we have demonstrated that the artifact symmetric signal arises from the leakage rf current in the oxide substrate, caused by the rf current shunting effect. We have further established a correlation between the magnitude of the artifact symmetric signal and the reactance of the capacitor formed in substrate through the GSG electrode. We have evaluated the influence of artifact symmetric signal on the spin-Hall ratio of Pt from oxide substrate with high relative permittivity (i.e., STO) by carrying out the ST-FMR and SHHV measurements, which indicates that the substrates with high relative permittivity significantly affect the evaluation of the spin-Hall ratio in the ST-FMR measurements. Our findings shed light on the critical influence of substrate-induced artifacts in ST-FMR measurements and highlight the importance of usage of suitable measurement techniques when studying spin-Hall source materials.

ACKNOWLEDGMENTS

This work was supported by the National Natural Science Foundation (Grants No. 52161135103, No. 52250418, No. 92163113), and Tsinghua University Initiative Scientific Research Program. W.S. acknowledges Grant No. 2021/40/Q/ST5/00209 (Sheng) from the National Science Centre, Poland.

[1] A. Manchon, J. Železný, I. M. Miron, T. Jungwirth, J. Sinova, A. Thiaville, K. Garello, and P. Gambardella, Current-induced spin-orbit torques in ferromagnetic and antiferromagnetic systems, Rev. Mod. Phys. **91**, 035004 (2019).

[2] X. Han, X. Wang, C. Wan, G. Yu, and X. Lv, Spin-orbit torques: Materials, physics, and devices, Appl. Phys. Lett. **118**, 120502 (2021).

[3] B. Dieny, *et al.*, Opportunities and challenges for spintronics in the microelectronics industry, Nat. Electron. **3**, 446 (2020).

[4] I. M. Miron, K. Garello, G. Gaudin, P.-J. Zermatten, M. V. Costache, S. Auffret, S. Bandiera, B. Rodmacq, A. Schuhl, and P. Gambardella, Perpendicular switching of a single ferromagnetic layer induced by in-plane current injection, Nature **476**, 189 (2011).

[5] K. Garello, F. Yasin, H. Hody, S. Couet, L. Souriau, S. H. Sharifi, J. Swerts, R. Carpenter, S. Rao, W. Kim, J. Wu, K. K. V. Sethu, M. Pak, N. Jossart, D. Crotti, A. Furnémont, and G. S. Kar, in *2019 Symposium on VLSI Circuits* (2019), pp. T194.

[6] Y. C. Wu, K. Garello, W. Kim, M. Gupta, M. Perumkunnil, V. Kateel, S. Couet, R. Carpenter, S. Rao, S. Van Beek, K. K. Vudya Sethu, F. Yasin, D. Crotti, and G. S. Kar, Voltage-gate-assisted spin-orbit-torque magnetic random-access memory for high-density and low-power embedded applications, Phys. Rev. Appl. **15**, 064015 (2021).

[7] W. Cai, K. Shi, Y. Zhuo, D. Zhu, Y. Huang, J. Yin, K. Cao, Z. Wang, Z. Guo, Z. Wang, G. Wang, and W. Zhao, Sub-ns field-free switching in perpendicular magnetic tunnel junctions by the interplay of spin transfer and orbit torques, IEEE Electron. Device Lett. **42**, 704 (2021).

[8] Q. Shao, P. Li, L. Liu, H. Yang, S. Fukami, A. Razavi, H. Wu, K. Wang, F. Freimuth, Y. Mokrousov, M. D. Stiles, S. Emori, A. Hoffmann, J. Åkerman, K. Roy, J. P. Wang, S. H. Yang, K. Garello, and W. Zhang, Roadmap of spin-orbit torques, IEEE Trans. Magn. **57**, 1 (2021).

[9] C. Safranski, J. Z. Sun, and A. D. Kent, A perspective on electrical generation of spin current for magnetic random access memories, Appl. Phys. Lett. **120**, 160502 (2022).

[10] S. V. Aradhya, G. E. Rowlands, J. Oh, D. C. Ralph, and R. A. Buhrman, Nanosecond-timescale low energy switching of in-plane magnetic tunnel junctions through dynamic Oersted-field-assisted spin Hall effect, Nano Lett. **16**, 5987 (2016).

[11] M.-H. Nguyen and C.-F. Pai, Spin-orbit torque characterization in a nutshell, APL Mater. **9**, 030902 (2021).
[12] L. Liu, T. Moriyama, D. C. Ralph, and R. A. Buhrman, Spin-torque ferromagnetic resonance induced by the spin Hall effect, Phys. Rev. Lett. **106**, 036601 (2011).
[13] T. Nan, S. Emori, C. T. Boone, X. Wang, T. M. Oxholm, J. G. Jones, B. M. Howe, G. J. Brown, and N. X. Sun, Comparison of spin-orbit torques and spin pumping across NiFe/Pt and NiFe/Cu/Pt interfaces, Phys. Rev. B **91**, 214416 (2015).
[14] T. Nan, *et al.*, Controlling spin current polarization through non-collinear antiferromagnetism, Nat. Commun. **11**, 4671 (2020).
[15] T. Nan, T. J. Anderson, J. Gibbons, K. Hwang, N. Campbell, H. Zhou, Y. Q. Dong, G. Y. Kim, D. F. Shao, T. R. Paudel, N. Reynolds, X. J. Wang, N. X. Sun, E. Y. Tsymbal, S. Y. Choi, M. S. Rzchowski, Y. B. Kim, D. C. Ralph, and C. B. Eom, Anisotropic spin-orbit torque generation in epitaxial $SrIrO_3$ by symmetry design, Proc. Natl. Acad. Sci. U. S. A. **116**, 16186 (2019).
[16] A. R. Mellnik, J. S. Lee, A. Richardella, J. L. Grab, P. J. Mintun, M. H. Fischer, A. Vaezi, A. Manchon, E. A. Kim, N. Samarth, and D. C. Ralph, Spin-transfer torque generated by a topological insulator, Nature **511**, 449 (2014).
[17] Y. Wang, P. Deorani, K. Banerjee, N. Koirala, M. Brahlek, S. Oh, and H. Yang, Topological surface states originated spin-orbit torques in Bi_2Se_3, Phys. Rev. Lett. **114**, 257202 (2015).
[18] M. Hayashi, J. Kim, M. Yamanouchi, and H. Ohno, Quantitative characterization of the spin-orbit torque using harmonic Hall voltage measurements, Phys. Rev. B **89**, 144425 (2014).
[19] U. H. Pi, K. Won Kim, J. Y. Bae, S. C. Lee, Y. J. Cho, K. S. Kim, and S. Seo, Tilting of the spin orientation induced by Rashba effect in ferromagnetic metal layer, Appl. Phys. Lett. **97**, 162507 (2010).
[20] L. Zhu, L. Zhu, and R. A. Buhrman, Fully spin-transparent magnetic interfaces enabled by the insertion of a thin paramagnetic NiO layer, Phys. Rev. Lett. **126**, 107204 (2021).
[21] I. H. Kao, R. Muzzio, H. Zhang, M. Zhu, J. Gobbo, S. Yuan, D. Weber, R. Rao, J. Li, J. H. Edgar, J. E. Goldberger, J. Yan, D. G. Mandrus, J. Hwang, R. Cheng, J. Katoch, and S. Singh, Deterministic switching of a perpendicularly polarized magnet using unconventional spin-orbit torques in WTe_2, Nat. Mater. **21**, 1029 (2022).
[22] H. Wu, S. A. Razavi, Q. Shao, X. Li, K. L. Wong, Y. Liu, G. Yin, and K. L. Wang, Spin-orbit torque from a ferromagnetic metal, Phys. Rev. B **99**, 184403 (2019).
[23] C.-F. Pai, M. Mann, A. J. Tan, and G. S. D. Beach, Determination of spin torque efficiencies in heterostructures with perpendicular magnetic anisotropy, Phys. Rev. B **93**, 144409 (2016).
[24] L. Zhu, D. C. Ralph, and R. A. Buhrman, Lack of simple correlation between switching current density and spin-orbit-torque efficiency of perpendicularly magnetized spin-current-generator-ferromagnet heterostructures, Phys. Rev. Appl. **15**, 024059 (2021).
[25] T. Xing, C. Zhou, C. X. Wang, Z. Li, A. N. Cao, W. L. Cai, X. Y. Zhang, B. Ji, T. Lin, Y. Z. Wu, N. Lei, Y. G. Zhang, and W. S. Zhao, Direct detection of spin-orbit effective fields through magneto-optical Kerr effect, Phys. Rev. B **101**, 224407 (2020).
[26] M. Montazeri, P. Upadhyaya, M. C. Onbasli, G. Yu, K. L. Wong, M. Lang, Y. Fan, X. Li, P. Khalili Amiri, R. N. Schwartz, C. A. Ross, and K. L. Wang, Magneto-optical investigation of spin-orbit torques in metallic and insulating magnetic heterostructures, Nat. Commun. **6**, 8958 (2015).
[27] B. Grover, B. K. Hazra, T. Ma, B. Pal, N. Bernstein, A. Rothschild, A. K. Srivastava, S. Choudhury, G. Woltersdorf, A. Capua, and S. S. P. Parkin, Crystallographic dependence of the spin Hall angle in epitaxial Pt films: Comparison of optical and electrical detection of spin-torque ferromagnetic resonance techniques, Appl. Phys. Lett. **120**, 172406 (2022).
[28] X. Huang, S. Sayed, J. Mittelstaedt, S. Susarla, S. Karimeddiny, L. Caretta, H. Zhang, V. A. Stoica, T. Gosavi, F. Mahfouzi, Q. Sun, P. Ercius, N. Kioussis, S. Salahuddin, D. C. Ralph, and R. Ramesh, Novel spin-orbit torque generation at room temperature in an all-oxide epitaxial $La_{0.7}Sr_{0.3}MnO_3/SrIrO_3$ system, Adv. Mater. **33**, 2008269 (2021).
[29] J. Zhou, X. Shu, W. Lin, D. F. Shao, S. Chen, L. Liu, P. Yang, E. Y. Tsymbal, and J. Chen, Modulation of spin-orbit torque from $SrRuO_3$ by epitaxial-strain-induced octahedral rotation, Adv. Mater. **33**, 2007114 (2021).
[30] J. Wei, H. Zhong, J. Liu, X. Wang, F. Meng, H. Xu, Y. Liu, X. Luo, Q. Zhang, Y. Guang, J. Feng, J. Zhang, L. Yang, C. Ge, L. Gu, K. Jin, G. Yu, and X. Han, Enhancement of spin-orbit torque by strain engineering in $SrRuO_3$ Films, Adv. Funct. Mater. **31**, 2100380 (2021).
[31] S. Karimeddiny, J. A. Mittelstaedt, R. A. Buhrman, and D. C. Ralph, Transverse and longitudinal spin-torque ferromagnetic resonance for improved measurement of spin-orbit torque, Phys. Rev. Appl. **14**, 024024 (2020).
[32] T. M. Cham, S. Karimeddiny, V. Gupta, J. A. Mittelstaedt, and D. C. Ralph, Separation of artifacts from spin-torque ferromagnetic resonance measurements of spin-orbit torque for the low-symmetry van der Waals semi-metal $ZrTe_3$, Adv. Quantum Technol. **5**, 2100111 (2022).
[33] J. Zhang, J. Zhang, X. Chi, R. Hao, W. Chen, H. Yang, D. Zhu, Q. Zhang, W. Zhao, H. Zhang, and J. Sun, Giant efficiency for charge-to-spin conversion via the electron gas at the $LaTiO_{3+\delta}/SrTiO_3$ interface, Phys. Rev. B **105**, 195110 (2022).
[34] H. Chen and D. Yi, Spin–charge conversion in transition metal oxides, APL Mater. **9**, 060908 (2021).
[35] A. Bose, J. N. Nelson, X. S. Zhang, P. Jadaun, R. Jain, D. G. Schlom, D. C. Ralph, D. A. Muller, K. M. Shen, and R. A. Buhrman, Effects of anisotropic strain on spin–orbit torque produced by the Dirac nodal line semimetal IrO_2, ACS Appl. Mater. Interfaces **12**, 55411 (2020).
[36] Y. Ou, Z. Wang, C. S. Chang, H. P. Nair, H. Paik, N. Reynolds, D. C. Ralph, D. A. Muller, D. G. Schlom, and R. A. Buhrman, Exceptionally high, strongly temperature dependent, spin Hall conductivity of $SrRuO_3$, Nano Lett. **19**, 3663 (2019).
[37] S. Hori, K. Ueda, T. Kida, M. Hagiwara, and J. Matsuno, Spin–orbit torque generation in bilayers composed

of CoFeB and epitaxial $SrIrO_3$ grown on an orthorhombic $DyScO_3$ substrate, Appl. Phys. Lett. **121**, 022402 (2022).

[38] H. Zhang, Z. Zhu, Y. Zhu, X. Chen, Q. Jiang, J. Wei, C. Zhao, J. Zhang, F. Han, H. Yang, D. Zhu, H. Wu, Y. Chen, F. Hu, B. Shen, W. Zhao, J. Zhang, G. Yu, and J. Sun, Fermi-level-dependent charge-to-spin conversion of the two-dimensional electron gas at the γ-$Al_2O_3/KTaO_3$ interface, Phys. Rev. Appl. **19**, 034045 (2023).

[39] E. Lesne, Y. Fu, S. Oyarzun, J. C. Rojas-Sánchez, D. C. Vaz, H. Naganuma, G. Sicoli, J. P. Attané, M. Jamet, E. Jacquet, J. M. George, A. Barthélémy, H. Jaffrès, A. Fert, M. Bibes, and L. Vila, Highly efficient and tunable spin-to-charge conversion through Rashba coupling at oxide interfaces, Nat. Mater. **15**, 1261 (2016).

[40] H. Zhang, Y. Ma, H. Zhang, X. Chen, S. Wang, G. Li, Y. Yun, X. Yan, Y. Chen, F. Hu, J. Cai, B. Shen, W. Han, and J. Sun, Thermal spin injection and inverse Edelstein effect of the two-dimensional electron gas at EuO-$KTaO_3$ interfaces, Nano Lett. **19**, 1605 (2019).

[41] R. C. Neville, B. Hoeneisen, and C. A. Mead, Permittivity of strontium titanate, J. Appl. Phys. **43**, 2124 (1972).

[42] V. Trepakov, V. Vikhnin, M. Savinov, P. Syrnikov, S. Kapphan, V. Lemanov, H. Hesse, and L. Jastrabik, Dielectric permittivity and Fe-and Cu-doping effect in $KTaO_3$ and $K_{1-x}Li_xTaO_3$, Ferroelectrics **235**, 59 (1999).

[43] J. Sinova, S. O. Valenzuela, J. Wunderlich, C. H. Back, and T. Jungwirth, Spin Hall effects, Rev. Mod. Phys. **87**, 1213 (2015).

[44] V. M. Edelstein, Spin polarization of conduction electrons induced by electric current in two-dimensional asymmetric electron systems, Solid State Commun. **73**, 233 (1990).

[45] D. MacNeill, G. M. Stiehl, M. H. D. Guimaraes, R. A. Buhrman, J. Park, and D. C. Ralph, Control of spin-orbit torques through crystal symmetry in WTe_2/ferromagnet bilayers, Nat. Phys. **13**, 300 (2017).

[46] Y. Wang, P. Deorani, X. Qiu, J. H. Kwon, and H. Yang, Determination of intrinsic spin Hall angle in Pt, Appl. Phys. Lett. **105**, 152412 (2014).

[47] Y. Fan, H. Li, M. Dc, T. Peterson, J. Held, P. Sahu, J. Chen, D. Zhang, A. Mkhoyan, and J.-P. Wang, Spin pumping and large field-like torque at room temperature in sputtered amorphous WTe_{2-x} films, APL Mater. **8**, 041102 (2020).

[48] K. Kondou, H. Chen, T. Tomita, M. Ikhlas, T. Higo, A. H. MacDonald, S. Nakatsuji, and Y. Otani, Giant field-like torque by the out-of-plane magnetic spin Hall effect in a topological antiferromagnet, Nat. Commun. **12**, 6491 (2021).

[49] See Supplemetary Material at http://link.aps.org/supplemental/10.1103/PhysRevApplied.21.024021 for more details about the measurements of impedance, evaluation of spin-Hall ratio of Si/SiO_2/Pt(5 nm)/Py(5 nm) sample, ST-FMR and SHHV results of different oxide substrate/Py devices, the derivation of ST-FMR mixing voltage of oxide substrate/Py device, ST-FMR and SHHV results of STO/Pt(5 nm)/Py(5 nm) and STO/Py(5 nm)/Pt(5 nm) samples, and ST-FMR results of STO/SIO(17 nm)/Py(5 nm) sample.

[50] C. Zuccaro, I. Ghosh, K. Urban, N. Klein, S. Penn, and N. M. Alford, Materials for HTS-shielded dielectric resonators, IEEE Trans. Appl. Supercond. **7**, 3715 (1997).

[51] V. Bovtun, M. Kempa, S. Kamba, V. Pashkov, V. Molchanov, Y. Poplavko, and Y. Yakymenko, in *IEEE XXXIII International Scientific Conference Electronics and Nanotechnology (ELNANO)* (2013), pp. 17–20.

[52] H. Birey, Thickness dependence of the dielectric constant and resistance of Al_2O_3 films, J. Appl. Phys. **48**, 5209 (1977).

[53] S. Emori, T. Nan, A. M. Belkessam, X. Wang, A. D. Matyushov, C. J. Babroski, Y. Gao, H. Lin, and N. X. Sun, Interfacial spin-orbit torque without bulk spin-orbit coupling, Phys. Rev. B **93**, 180402(R) (2016).

[54] T. Seki, Y. Lau, S. Iihama, and K. Takanashi, Spin-orbit torque in a Ni-Fe single layer, Phys. Rev. B **104**, 094430 (2021).

[55] A. Tsukahara, Y. Ando, Y. Kitamura, H. Emoto, E. Shikoh, M. P. Delmo, T. Shinjo, and M. Shiraishi, Self-induced inverse spin Hall effect in permalloy at room temperature, Phys. Rev. B **89**, 235317 (2014).

[56] L. M. Vicente-Arche, *et al.*, Spin-charge interconversion in $KTaO_3$ 2D electron gases, Adv. Mater. **33**, 2102102 (2021).

[57] A. Tang, T. Xu, S. Liu, Y. Liang, H. Chen, D. Yan, Y. Shi, P. Yu, R. Yu, and Y. Lin, Implementing complex oxides for efficient room-temperature spin–orbit torque switching, Adv. Electron. Mater. **8**, 2200514 (2022).

[58] D. Zheng, J. Lan, B. Fang, Y. Li, C. Liu, J. O. Ledesma-Martin, Y. Wen, P. Li, C. Zhang, Y. Ma, Z. Qiu, K. Liu, A. Manchon, and X. Zhang, High-efficiency magnon-mediated magnetization switching in all-oxide heterostructures with perpendicular magnetic anisotropy, Adv. Mater. **34**, 2203038 (2022).